Swelling Heterogeneities in End-Linked Model Networks: A Combined Proton Multiple-Quantum NMR and Computer Simulation Study

Kay Saalwächter* and Felix Kleinschmidt

Institut für Makromolekulare Chemie, Universität Freiburg, Stefan-Meier-Str. 31, D-79104 Freiburg, Germany

Jens-Uwe Sommer

Institut de Chimie des Surfaces et Interfaces (CNRS), 15, rue Jean Starcky, F-68057 Mulhouse Cedex, France

Received June 17, 2004; Revised Manuscript Received September 6, 2004

ABSTRACT: The segmental order of monomodal and bimodal polymer networks is investigated by proton multiple-quantum NMR spectroscopy as applied to poly(dimethylsiloxane) model systems and by Monte Carlo simulations using the bond fluctuation model. The multiple-quantum method is sensitive to chain order parameter distributions and therefore probes heterogeneities in the extent of fast motional averaging of individual network strands subject to topological constraints. These data are in qualitative agreement with the simulations. We find a broadening of the chain order parameter distribution upon swelling accompanied by a nonaffine change of this distribution, indicating a heterogeneous swelling process. Comparing the simulated tensor order parameter with the autocorrelation function of segments, we observe major deviations in the swollen state but also for the long-chain fraction of the dry, bimodal network. These effects are attributed to the fluctuation dependence of the tensor order parameter which comprises information about both orientational order as well as fluctuation properties of fast segment reorientation processes. In general, our results indicate that segmental order is not simply related to the cross-link density. Fluctuations on larger scales such as reorientation of chain clusters, dynamical correlations between segments in the entangled state, and heterogeneities in the segmental fluctuations have an essential influence on the tensorial order. The spatial length scale of the heterogeneities is also investigated by self-diffusion measurements of the solvent molecules.

I. Introduction

After more than 60 years of active research, the swelling of polymer networks is still not well understood on a molecular scale. While the early, affine theory developed by Flory and Rehner[1] is still enjoying great popularity when cross-link densities are to be determined by equilibrium swelling,[2] serious discrepancies have been identified in particular at lower swelling.[3−5] The central observation was that the so-called reduced dilation modulus, which reflects the normalized propensity of a network to take up solvent (as measured by its chemical potential) in comparison to a melt composed of the equivalent, non-cross-linked network chains, goes through a maximum instead of exhibiting monotonic behavior. Gottlieb and Gaylord[4] found that the maximum cannot satisfactorily be explained by any current theory and concluded that the discrepancies are most probably related to a violation of the assumption of separability of elastic and mixing contributions to the total free energy.

At around the same time, Bastide et al.[6,7] as well as Ullman[8] pointed out that thermodynamic anomalies in the swelling of networks with controlled amounts of pendant chains and also earlier observations from scattering experiments concerning surprisingly weak changes in the overall radius of gyration of the network chains upon swelling might be explainable in terms of a dominance of topological rearrangements ("desinterspersion") at the early stages. Swelling should further enhance the observation of heterogeneities in the cross-link density resulting from concentration fluctuations frozen-in upon cross-linking. These are manifested in the notable excess scattering of swollen networks compared to semidilute solutions observed at low **q** in X-ray,[9] neutron,[10−12] and static[13] and dynamic light scattering in nonergodic samples.[14] A recent paper[15] demonstrated that heterogeneities in poly(*N*-isopropylacrylamide) networks might even reach the micron range and can thus be visualized using real-space confocal microscopy techniques.

On the theoretical side, there is an ongoing dispute about the role of nonaffine deformations and the effect of network topology on larger scales. Recent work has taken up the ideas of swelling heterogeneities and nonaffine topological rearrangements.[16−20] Panyukov and Rabin showed that their replica mean-field theory is able to predict the famous "butterfly pattern" that was earlier observed in neutron scattering on stretched swollen networks and attributed to swelling heterogeneities.[10] Sommer et al. focused on the role of topological rearrangements on the swelling process, using analytical arguments as well as computer simulations.[18−20] Computer simulations are a particularly important instrument for a complementary analysis of experiments, as in the latter, structural information on conformational changes of topologically connected parts is generally not available. Simulations in turn provide access to local details, including topological effects. For a review about early simulations of network swelling we refer to the work of Escobedo and de Pablo.[21] Pütz, Kremer, and Everaers[22] have studied the swelling behavior of randomly cross-linked networks using molecular dynamics. These authors found nonaffine defor-

* Corresponding author. E-mail kays@makro.uni-freiburg.de.

10.1021/ma048803k CCC: $27.50
Published on Web 10/21/2004

mation of network stands during swelling in accordance with previous work.[23−25] For a discussion of the deformation model proposed in their work, see also ref 20.

As a certain limitation in simulation studies, one has to deal with long time scales of relaxation processes which involve large-scale nonaffine rearrangements. Only simulation techniques which efficiently bridge the length scales from the smallest relevant units (usually statistical segments) to mesoscopic behavior as well as time scales from segmental diffusion up to cooperative rearrangement processes can be seriously considered for simulation of polymer networks. As such, lattice Monte Carlo methods like the bond fluctuation model (BFM) are among the best candidates. Even then, simulation times of several months (on fast PC-type hardware) are to be expected for a single network. Here, we extend our earlier investigations using the bond fluctuation model (BFM) applied to the swelling of bimodal networks[20] to calculations of order parameters, which play a key role in NMR observables.

NMR, being complementary to scattering methods, represents a tool of major importance for the molecular-scale investigation of order and dynamics in polymer systems.[26] In particular, the analysis of transverse relaxation phenomena in polymers at temperatures far above T_g provides semilocal structural information. This is realized by the orientation dependence of dipole−dipole or quadrupolar interactions of nuclear spins with respect to the outer magnetic field. Rapid molecular motion of spins associated with the monomer unit in a polymer leads to an averaging of these interactions, which (in contrast to small-molecule liquids) is not isotropic. Residual tensorial interactions[27,28] originate from imperfect motional averaging of chain segments fluctuating rapidly between topological constraints such as cross-links or chain entanglements and exert an influence on the NMR response of the system. The size scale of hindered subchains becomes thus accessible. Residual couplings may reach a magnitude of several percent of the corresponding static interaction and are directly proportional to a dynamic order parameter of the polymer backbone, S_b, which lends itself to comparisons with theory. The concept was previously applied to the investigation of network swelling,[29−31] and observations on the evolution of network chain order were consistently interpreted in terms of chain desinterspersion.[32]

The effect of swelling heterogeneity, however, eluded NMR analysis until now. This is probably due to the strong model assumptions employed in the interpretation of rather featureless transverses relaxation data.[33,34] Progress concerning a more precise measurement of proton residual dipole−dipole couplings was reported for the combination of Hahn and solid echo-type experiments.[28,35−38] Recently, we have introduced a robust strategy based on proton multiple-quantum (MQ) spectroscopy.[39−41] These methods are among the most recent and versatile experiments which provide information on local chain order in polymers.[42,43] With our new approach, we succeeded in quantifying even chain order distributions, i.e., molecular-scale heterogeneity, in network samples,[39] and further showed that the method can be implemented on low-cost low-field instrumentation with hardly any compromise on the accuracy.[41]

We here report on an application to partially swollen, end-linked poly(dimethylsiloxane) networks. Preliminary results concerning the sensitivity of our method to swelling heterogeneities were already communicated.[41] We now present a detailed study of networks which are composed of precursor chains of varying length and of bimodal mixtures of very short and long chains. Heterogeneities are found upon swelling of all these systems, and the shapes of order parameter distributions change in a characteristic fashion. NMR and computer simulation results are found to be in convincing qualitative agreement, which concerns in particular the nonaffinity of the changes. In addition, order parameters extracted from computer simulations reveal new insights into the relation between NMR observables and network properties, which particularly concern the influence of fluctuations on the tensor order parameter governing the NMR response. We therefore provide an in-depth discussion of the differences observed in analyzing the simulations in terms of simple bond orientation and tensorial order. Finally, we have attempted to investigate the length scale of topological changes upon swelling, as potentially reflected in the time and concentration dependence of the self-diffusion coefficient of the solvent molecules.

The rest of this work is organized as follows: In section II we present details about the samples, the experimental approaches, and the simulation method. Our results are reported and interpreted in sections IIIA−C and are compared and discussed in section IV. A summary of this work is given in section V.

Table 1. Investigated Mono- and Bimodal PDMS Model Networks Composed of Long (M_n = 47 200 g/mol, PD = 1.64), Medium (M_n = 5200 g/mol, PD = 1.86), and Short (M_n = 780 g/mol, PD = 1.49) Chains

	% w/w sol[a]	Q_{eq}[b]	E (MPa)[c]	N[d]
net800	2.7	1.9	4.85	2
net5k	4.2	3.1	1.3	12
net47k	7	5.2	0.8	109
netb30[e]	5.0	3.1	1.5	$\langle N \rangle = 6.4$

[a] Determined by swelling experiments in toluene. [b] Equilibrium degree of volume swelling ($1/\phi_V$) in toluene. [c] Young's modulus as measured by uniaxial extension. [d] Number of (Kuhn) segments between cross-links, estimated from M_n using $C_\infty = 5.85$.[44] [e] The bimodal network, netb30, consists of 70% w/w long and 30% short chains.

II. Experimental Section

Samples. Experiments are carried out on mono- and bimodal poly(dimethylsiloxane) (PDMS) networks prepared from linear hydroxyl-terminated precursor polymers (Gelest) using tetraethoxysilane as cross-linker. The synthesis and characterization of the samples are described in ref 39, and key properties are summarized in Table 1.

The networks are characterized by a very good conversion of precursor chain ends, yielding very low sol contents as well as low amounts of dangling chains, as shown previously using the MQ NMR method.[39] In this work, the order parameter distributions of three of the four samples were investigated in the dry state. The bimodality found earlier for the order parameter distributions of bimodal networks served as a benchmark for the sensitivity of the NMR method to such distributions.

For the present work, the samples are swollen in octane, chosen due to its low volatility. It is a good solvent for PDMS.[45] Different protocols have been tested, such as direct mixing, swelling in octane vapor, and gradual swelling in different mixtures of ethanol and octane. In this way, we ensure that the observed effects of heterogeneity are not a function of preparation conditions, where rapid swelling could lead to chain scission and development of microscopic cracks. To reach

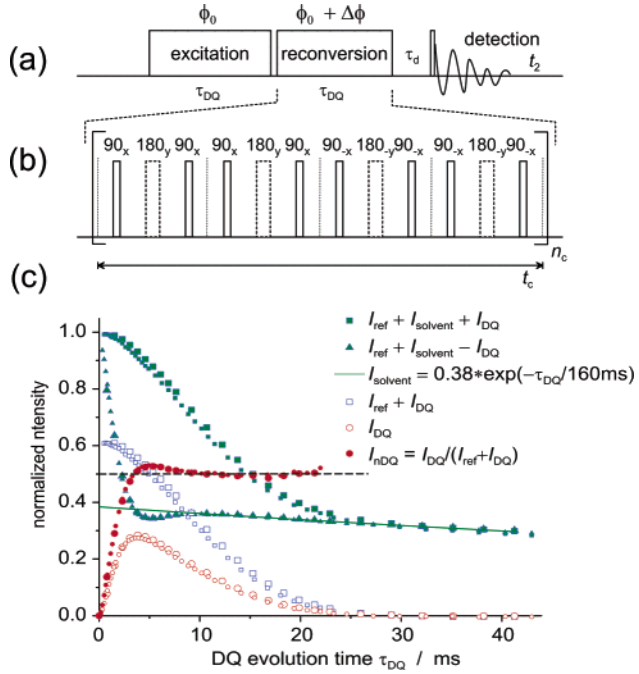

Figure 1. (a) Scheme of the multiple-quantum experiment used in this work,[39] (b) the specific pulse sequence block,[48] and (c) data for net47k at $Q = 1.4$. Experimental intensities are scaled to the full intensity of a one-pulse spectrum. Large and small symbols are from experiments with sequence cycle times t_c of 200 and 800 μs, corresponding to pulse duty cycles of 24% and only 6%, respectively. The expected intensity plateau of the normalized DQ intensity is indicated by the dashed line.

a specific degree of swelling, Q_w (given in terms of $m_{swollen}/m_{dry} = 1 + m_{octane}/m_{PDMS}$), swollen samples are placed on a balance, and when the desired weight is attained by evaporation after several minutes, samples are transferred into 4 mm magic-angle spinning rotors and closed with KelF caps, thus establishing a swelling equilibrium with the solvent vapor pressure. The tightness of the caps is checked regularly by measuring potential weight loss. The same sample vessels are used for the MQ as well as the diffusion NMR measurements. The degree of volume swelling, denoted as Q, is linearly related to $(Q_w - 1) = m_{octane}/m_{PDMS}$ through simple additivity of volumes:[30] $Q = 1 + (\rho_{PDMS}/\rho_{octane})(Q_w - 1) = 1 + 1.4(Q_w - 1)$.

NMR Spectroscopy. The response of polymeric networks or melts in proton NMR experiments is commonly analyzed in terms of residual dipolar interactions.[27] These originate from imperfect motional averaging of chain segments fluctuating between topological constraints such as cross-links or chain entanglements and may reach a magnitude of several percent of the corresponding static interaction. Residual interactions are directly proportional to a dynamic order parameter of the polymer backbone

$$S_b = \frac{D_{res}}{D_{stat}} \frac{1}{\overline{P_2(\cos\alpha)}} = \frac{3}{5}\frac{r^2}{N} \qquad (1)$$

and can be calculated from the residual dipolar coupling constant, D_{res}, by comparison with its static counterpart, D_{stat}. α is the orientation of the internuclear coupling vector with respect to the segmental orientation. As indicated by the right-hand side of eq 1, S_b is related to r, the ratio of the end-to-end vector to its average, unperturbed melt state ($r^2 = \mathbf{r}^2/\overline{\mathbf{r}_0^2}$), and to N, the number of statistical chain segments between the constraints.[46] The measurement of D_{res} therefore provides information on the cross-link density[47] and should be related to microscopic stretching that is expected when the sample is isotropically dilated upon swelling.

A pulse scheme of the ^{1}H MQ experiment used herein is depicted in Figure 1a,b. It embodies the application of a specific double-quantum (DQ) excitation pulse sequence (b) of variable duration τ_{DQ},[48] along with a phase cycle over $\Delta\Phi$, by which a DQ-filtered (I_{DQ}) and a reference (I_{ref}) intensity can be measured. I_{DQ} subsumes signal from dipolar coupled segments and all $4n + 2$ quantum orders (as a result of the four-step selection phase cycle). I_{ref} contains contributions from all $4n$ quantum orders as well as dipolar-encoded longitudinal magnetization plus all signal from uncoupled, i.e., isotropically mobile components (solvent in the case of swollen systems, sol, dangling chains). The sum of these two contributions comprises the full magnetization of the sample subject to relaxation and is used to normalize the DQ-filtered intensity. Before doing so, uncoupled contributions which appear as very slowly relaxing tails of I_{ref} must be subtracted. The procedure is shown in Figure 1c. The tails are most reliably identified in a plot of $I_{ref} - I_{DQ}$.[49] The "coupled" intensity is distributed evenly among I_{ref} and I_{DQ} once the plateau of the buildup is reached, such that from this time on the intensity difference is composed only of uncoupled contributions.

We have shown that long-time relaxation of the overall coupled signal is mainly due to slow, cooperative motions of topological constraints and that signal decay due to experimental imperfections can safely be neglected.[40] This is also apparent from Figure 1, where data from experiments with very different pulse duty cycles are compared. Note that DQ buildup is usually complete within a time during which the sum intensity has decayed by less than 20%. The DQ buildup can therefore be analyzed in terms of residual dipolar couplings only. Other effects (influence of slow motions in particular) are negligible. This constitutes the major advantage of MQ spectroscopy over the more traditional relaxation experiments, in which rather strong models involving decay due to slow motions have to be invoked for analysis and in which decay due to nondipolar effects (e.g., diffusion in local field gradients) cannot be separated.

The normalized DQ buildup data are temperature-independent over tens of kelvin, providing further evidence that slow-motional effects are largely absent in I_{nDQ}. Using only intensities $I_{nDQ} \leq 0.45$, the normalized DQ buildup curves are analyzed with a monomer-specific buildup function[39]

$$I_{nDQ} = 0.5(1 - \exp\{-31.91(D_{res}/2\pi)^2\tau_{DQ}^2\}) \qquad (2)$$

here given for poly(dimethylsiloxane) (PDMS). $D_{res}/2\pi$ and τ_{DQ} are in kHz and ms, respectively. Fits restricted to the initial part of the DQ buildup ($I_{nDQ} \leq 0.2$) are also performed, with the result denoted as $D_{initial}$. Another fitting function assuming a Gaussian distribution of D_{res} is given in ref 39, and yields an average coupling constant as well as a standard deviation (reported as D_G and σ_G, respectively). Finally, eq 2 is also used as the kernel function in a regularization procedure used to determine distribution functions of D_{res} in a numerically stable way. The algorithm, called fast Thikonov regularization (FTIKREG), was published by Weese.[50] It features an automatic (and conservative) determination of the regularization parameter based on the estimated error limits and thus biases potential distributions toward less maxima. Error intervals for the amplitudes associated with the fixed bins of D_{res} as given by the algorithm amount to about 10% of the maximum amplitude. Average coupling constants as well as the standard deviations are also calculated from the so-obtained distributions and are denoted as D_{reg} and σ_{reg}.

Further details on the experimental procedure and an in-depth discussion of the limits of the method may be taken from ref 39. From the experimental dipolar coupling constants, the backbone order parameters are readily calculated using eq 1 with $D_{stat}/2\pi = 8.9$ kHz and $\alpha = 90°$. Experiments are performed on a Bruker Avance 500 solid-state NMR spectrometer ($B_0 = 11.7$ T) using the proton channel of a commercial static double-resonance probe (^{1}H 90° pulses of 3 μs length) as well as a Bruker minispec mq20 operating at 0.5 T (1.9 μs 90° pulses). At high field, the n_c-incremented version of the MQ experiment with cycle times of $t_c = 200$ and 800 μs is used (providing rapid refocusing of shift and susceptibility effects,

Table 2. Essential Properties of the Simulated Networks[a]

property	monomodal	bimodal
lattice	200 × 200 × 200, cubic	200 × 200 × 200, cubic
boundaries	reflecting (solid walls)	reflecting (solid walls)
lattice occupation	0.5 melt, 0.51 cross-linked	0.5, 0.5125
short chains in bond units		$N_S = 4$, $n_S = 21,060$
long chains in bond units	$N = 24$, $n = 20,000$	$N_L = 99$, $n_L = 3,947$
averaged strand length in bond units (loop-reduced)	$\langle N \rangle = 26$	$\langle N \rangle = 25$
volume fraction of short chains		$c = 0.21$
mole fraction of short chains		$p = 0.84$
number of cross-links	$n_C = 10,000$	$n_C = 12,504$
functionality	$f = 4$, $\langle f \rangle = 3.9$	$f = 4$, $\langle f \rangle = 3.9$
gel fraction	$c_{gel} = 0.995$	$c_{gel} = 0.985$
mean squared bond length b^2	6.92 (dry), 7.49 (swollen)	6.92 (dry), 7.5 (swollen)
swelling degree Q	5.2	5.5

[a]Notation: N_X = length of X-chains, n_X = number of X-chains, c = volume fraction of short chains, p = mole fraction of short chains, f = functionality of cross-links, and c_{gel} = gel fraction.

thus also suppressing the influence of isotropic J couplings), while on the minispec, the time-incremented two-cycle version ($n_c = 2$) is the more robust choice.

Pulsed-field gradient measurements of the self-diffusion coefficient of the solvent, D_{self}, are performed in a Bruker high-resolution-type probe with a singly tuned saddle coil (~5 μs 90° pulses) equipped with the Bruker Micro5 imaging system using the pulsed gradient stimulated-echo[51] technique (PG-STE). The diffusion delay Δ is varied between a minimum duration of 10 ms and a maximum of 3000 ms. Trapezoidal gradient shapes of 1.5 ms length are employed for encoding and decoding, and an additional burst gradient is applied during the diffusion delay Δ. Each acquisition is preceded by a train of gradient pulses of matched amplitude and timing in order to ensure reliable gradient power. The measurement temperature is fixed at 24 °C and controlled via the gradient cooling system, which has turned out to be the most reliable method to minimize the influence of convection. Summed solvent signal intensities are analyzed using the well-known relation[52]

$$\ln \frac{I}{I_0} = -4\pi^2 q^2 D_{self}(\Delta - \delta/3) \qquad (3)$$

where a correction for the finite duration of the gradient pulses, δ, is included. The wave vector $q = \gamma_H \delta g/(2\pi)$ further depends on the magnetogyric ratio, γ_H, and the gradient, g. A constant contribution from the broad, underlying network signal is taken into account.

Computer Simulations. Using the bond fluctuation model (BFM),[53] we simulate end-linked monomodal and bimodal networks. The networks are created in three steps: Before cross-linking, the simulation boxes of size 200 × 200 × 200 contain equilibrated melts with a lattice density of $\phi = 0.5$ (500 000 monomers in both cases). This density corresponds to a dense melt in the framework of the BFM.[54] The monomodal system contains chains with 25 repeat units (24 bonds), while the bimodal system contains long chains of 100 repeat units (99 bonds) and short chains of 5 repeat units (4 bonds). The monomer fraction of short chains is 21%. In the following we will exclusively use bond units, denoted as N, which are more suitable in the context of segmental order parameters. These numbers may be compared with the length of the experimentally investigated network precursors given in terms of Kuhn segments (Table 1).

In a second step, 4-functional cross-linker units are randomly attached to ends of the chains. The number of cross-linkers exactly obeys the necessary stoichiometric fraction; no excess (as in real synthesis) is used. In the third step, the cross-linkers are allowed to form new permanent bonds to free chain ends. A new bond is formed if a free chain end and a cross-linker (which must have at least one free radical) come into contact during the course of their motion. We only use local moves for all the results presented in this work. The time unit is one Monte Carlo Step (MCS), which corresponds to an attempted Monte Carlo move for each monomer. Note that due to the formation of new bonds the strand length is increased by two bond units compared to the free chains. This is taken into account in all N-dependent theoretical calculations below.

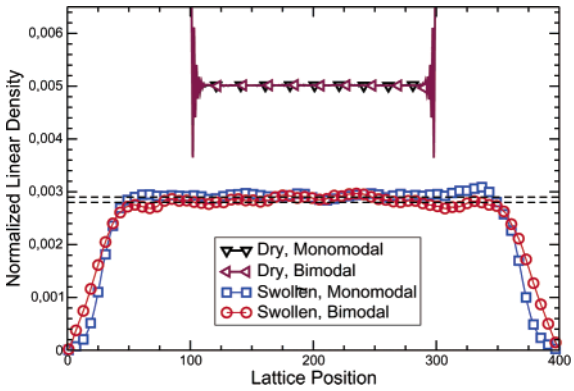

Figure 2. Density profiles before and after swelling. The linear density of the purified part (without loops and tails) is plotted as a function of the x-coordinate of the simulation box both for the dry (upper part) and for the swollen networks (lower part). The averaged densities of the swollen networks are indicated as dashed lines.

The gel fraction obtained for the monomodal (bimodal) network is 0.995 (0.9854). The bimodal network is assembled such that the short chains are nearly diluted within the long chains while the short chains provide the majority of reactive chain ends. Upon cross-linking, the subsystem of short chains becomes unstable with respect to its density distribution and forms a heterogeneous subnetwork within a matrix of long chains.[20] The essential data for the simulated networks are displayed in Table 2. More details can be found in ref 20.

Swelling with athermal solvent (free lattice sites) is initiated by expanding the size of the simulation box. For both networks, we have enlarged the simulation box by a factor of 2 in all directions. Hence, a maximum degree of swelling, $Q_{max} = 8$, could be achieved. The swelling ratio Q is defined as the ratio between the volume fraction of the network before and after swelling. During our simulations (up to 80 000 000 MCS), swelling equilibrium is nearly reached. This takes about half a year of simulation time. In Figure 2, we display the linear density profile for both networks before and after swelling. The overall swelling behavior is very similar for both networks. The monomodal network displays a swelling ratio of $Q = 5.2$ while for the bimodal network $Q = 5.5$. These values have been obtained by direct calculation of the density of the purified part (gel fraction without loops and dangling ends) in the center of the simulation box (80 × 80 × 80 lattice units) before and after swelling. The corresponding linear swelling degrees are indicated as dashed lines in Figure 2.

During the process of network formation, the short chains in the bimodal network form 27% self-loops. Taking into account only the loop-reduced fraction of chains, we obtain an average strand length of $\langle N \rangle = 25$ for the bimodal network.

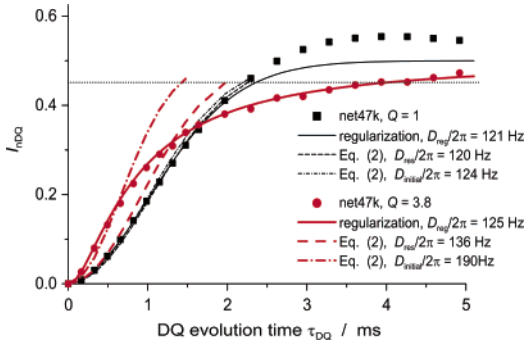

Figure 3. Normalized DQ buildup curves of dry and swollen net47k, along with results of the various fitting procedures. The dashed horizontal line indicates the intensity up to which data points were considered for fitting.

The monomodal system also contains 5% loops, which, however, do not have direct impact on the averaged network chain length. Because of the additional bonds formed, we obtain $\langle N \rangle = 26$ in this case. Chain elongation by end-linking is very rare and can be neglected. Therefore, from the point of view of local composition, both system are comparable.

III. Results

A. Chain Order by Multiple-Quantum NMR. Typical normalized DQ buildup curves for a dry and a swollen sample of net47k and results of their analysis are plotted in Figure 3. These results are prototypical for our observation of swelling heterogeneity which was already reported in a previous communication:[41] The buildup curve of the dry network is indicative of a rather narrow order parameter distribution. This is corroborated by the good agreement between fits to the whole buildup for $I_{nDQ} \leq 0.45$, to the initial rise only, and the result from regularization. It should be mentioned that the corresponding distribution of couplings is significantly narrower than predicted by established models,[55] which usually assume a Gaussian distribution of end-to-end distances of network chains, leading to a rather broad Γ-distribution of residual couplings.[39] Upon swelling, the order parameter distribution broadens significantly, as is immediately perceived from the shape change of the buildup curve.

Consistently, only the initial rise can be represented by eq 2 while the whole buildup function is not adequately described by a single-component model. While a fraction of chains are apparently stretched and acquire a higher order parameter than in the dry state, other chains or chain segments are even relaxed. We interpret this as a clear signature of swelling as being a complex nonaffine topological unfolding process, with these NMR data probably being the most direct molecular scale evidence to date. Note that, according to eq 1, affine swelling would lead to a simple affine scaling of the buildup curve along the x-axis by $Q^{-2/3}$.

Results of our systematic investigations of four different network samples at various degrees of swelling are summarized in Figures 4 and 5. Figure 4 demonstrates the universality of the phenomenon of a broad-

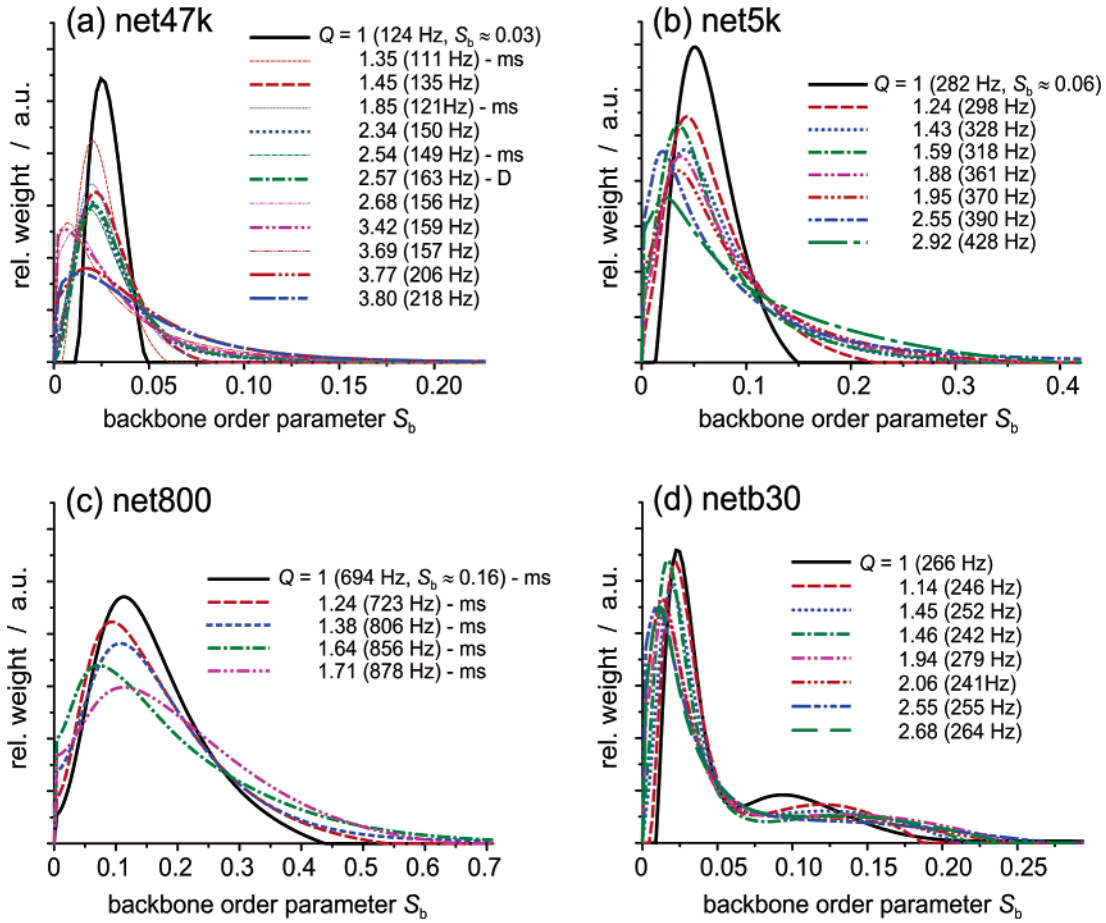

Figure 4. Order parameter distributions, determined by regularization analysis of DQ buildup data for four different networks at various degrees of swelling, Q. The numbers in brackets are the average residual dipolar coupling constants calculated from the distributions. In (a) and (c), "ms" denotes data from experiments performed with the minispec and "D" indicates a swelling experiment using deuterated octane, for which the correction for liquidlike components (tail subtraction) was not necessary.

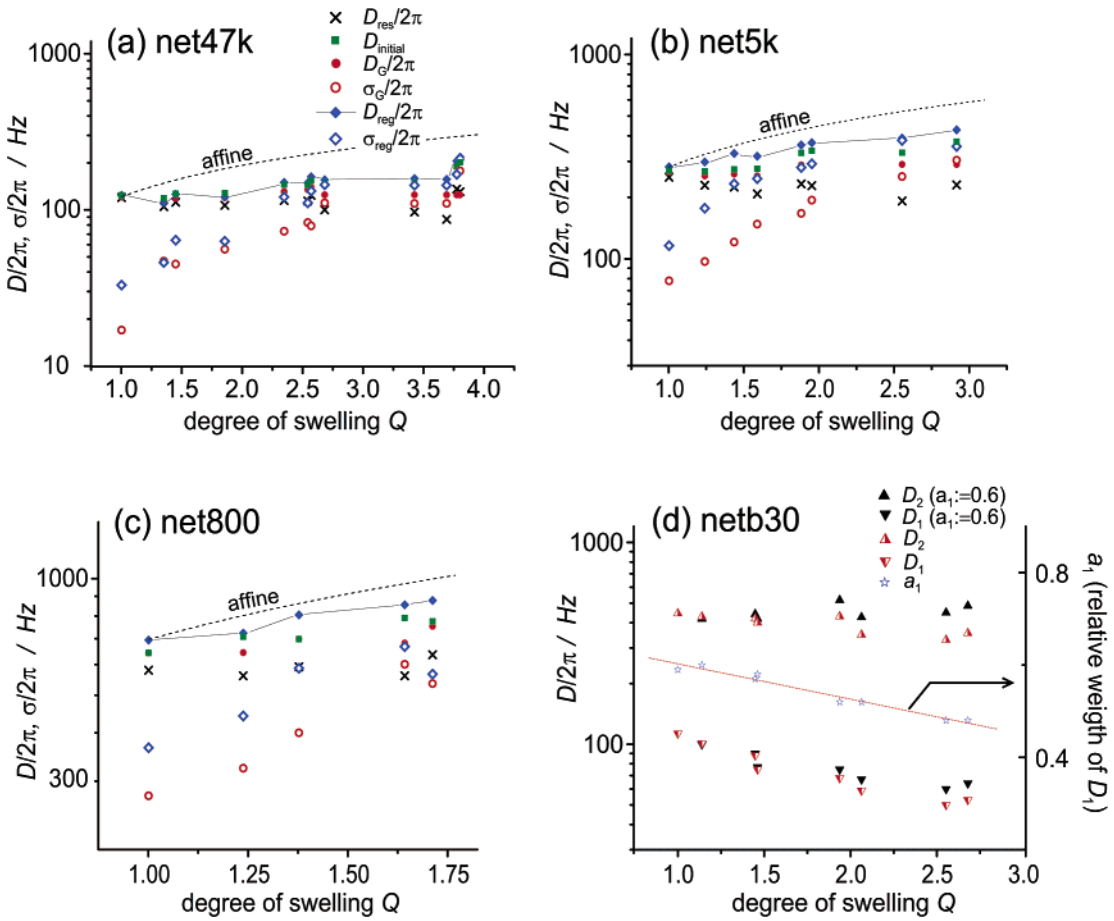

Figure 5. Residual dipolar couplings and widths of their distributions as determined by the different fitting procedures described in the text. Data are plotted for the four different networks (a−d), where in (a−c) the dashed line indicates the prediction for D_{reg} based on affine stretching. For the bimodal network netb30 (d), only a two-component model (two terms equal to eq 2, with a relative weighting factor a_1) was used. In this case, fitting was performed with all three parameters free as well as with the relative weight fixed at the value $a_1 = 0.6$ found for the dry sample.

ening of order parameter distributions upon swelling. The four networks differ widely in their relative cross-link densities. Yet, in all samples we observe the same trend of broadening of the distribution upon swelling, with a tendency of the maximum of the distribution to shift slightly to lower order. This is a clear indication of a subaffine process (vide infra). The average order parameters of these distributions exhibit only a weak trend toward higher values.

Basically the same information can be taken from Figure 5, in which the results from evaluations of the distributions in Figure 4 as well as results from other fits are compiled. Average order parameters increase only slightly upon swelling while the widths of the distributions increase notably. Generally, regularization analysis yields higher values for σ (width of distribution), presumably because the Gaussian fit does not capture the correct shape of the distributions. Note that the Gaussian fit becomes unstable once σ_G reaches the same order of magnitude as D_G. In such cases, the best fit converges to $D_G = 0$. To avoid this unphysical result and obtain comparable data for σ_G, D_G was kept fixed at the value obtained for the one more weakly swollen sample for which the fit was still stable.

To highlight the deviations from affine theory, we have plotted affine predictions derived from eq 1, using volume additivity

$$D_{reg}(Q) = D_{reg}(0)Q^{2/3} \qquad (4)$$

as dashed lines in Figure 5a−c. Subaffinity is clearly apparent, with a notable trend toward less serious discrepancies as the average strand length is decreased. Deviations of the average NMR chain order from the affine prediction have been observed before and are discussed below.

The distribution analysis of the bimodal network (Figure 4d) is interesting in that, owing to the large difference in chain length between the two components of netb30, it is possible to resolve these by their respective order parameters using the regularization procedure. Upon swelling, the regularization still yields two-component distributions, and it appears attractive to interpret changes in these two components in terms of differential swelling. The long-chain components seem to be relaxed upon swelling, while the maxima observed at higher order parameters attributed to the short-chain component in the dry network shift to somewhat higher order.

The apparent mobility increase of long chains is also corroborated by the fitting results (Figure 5d), where a three-parameter, two-component model based on eq 2 is the only model that yields numerically stable results. For instance, using a two-component model with one or two components being Gaussian-distributed (four or five parameters), the overall quality of the fit improves (naturally), however, at the expense of multiple stable minima, some with the unphysical result $D_{1/2} = 0$. From the comparison of three-parameter fits with free and

fixed relative amplitudes of short and long chains, we conclude that a fraction of long chains with increased order might actually enter the average value of the more strongly coupled fraction, D_2, for which we do not observe the trend toward increasing values inferred from the distributions. This caveat may also apply for the regularization analysis, for which a clean separability of a complex distribution into distinct components is limited by systematic errors on the 10% scale. In addition, even the pure long-chain network is seen to develop a considerable contribution of highly ordered chains (Figure 4a). The decrease of D_1, however, is a reliable observation as D_1 still decreases even when its relative amplitude is fixed at 60%.

B. Solvent Diffusion. PGSTE diffusion measurements are performed in order to evaluate a possible influence of heterogeneities in the swollen networks on the self-diffusion coefficient of the solvent. Results from recent literature suggest that swelling heterogeneities might even reach the micrometer scale[15] and thus become detectable by PFG NMR. Given sufficient diffusion contrast between more or less swollen regions, one would expect a diffusion time (Δ) dependence of an apparent D_{self} when the experimentally variable diffusion length, $\sqrt{D_{self}\Delta}$, reached the length scale of the heterogeneities.[56]

$\sqrt{D_{self}\Delta}$ changes between 2 and 70 μm in our experiments, and in this range, no appreciable variation of D_{self} was found. A weak Δ dependence was reported in studies of swollen natural rubber[57] and polystyrene gel beads.[58] In the latter case, anomalies were even detected in terms of deviations of the intensity data from the gradient strength variation as described by eq 3. Such effects are not expected for diffusion within fractal structures. Note that in both of these studies the pulsed-gradient spin-echo (PGSE) technique, which features free spin evolution during Δ, was used. Our results from PGSE experiments (not shown) exhibit a substantial dependence on Δ with up to 40% reductions in D_{self} at high Q when comparing data acquired with $\Delta = 5$ and 100 ms. Since we found no indication of this phenomenon using PGSTE, we concluded this effect to be an artifact, the origin of which is unclear to us.

Still, even much smaller local variations in solvent diffusivity could lead to different dependencies of D_{self} on Q when different samples are compared.[59] We expected that, in particular at low swelling, percolation structures of higher swollen regions could form at different Q in our vastly different samples. However, this was also not the case, at least not within the accuracy of our data (see Figure 6). Therefore, the diffusivity contrast between differently swollen regions is either too low or the length scale associated with the heterogeneity observed for the chain order phenomenon is simply too small to be detected by rapidly diffusion solvent molecules.

C. Chain Order by Computer Simulations. Chain order is most intuitively reflected in the autocorrelation function for each bond vector in the simulated networks. It is defined as

$$m(t) = \frac{[\mathbf{b}(0)\,\mathbf{b}(t)]}{[\langle b^2\rangle]} \tag{5}$$

where $\mathbf{b}(t)$ denotes the bond vector at time t. Structural averaging over a given *set* of bond vectors belonging to different types of network chains is denoted as [...]. In the denominator, also time averaging, denoted as $\langle ... \rangle$, is introduced, since thermal equilibrium (at least on the level of bond vector orientation) can be assumed. The long-time limit of the correlation function, $m = m(t \to \infty)$, is referred to as residual orientational order parameter of the bonds, which should be related to the experimental S_b (eq 1). We then write

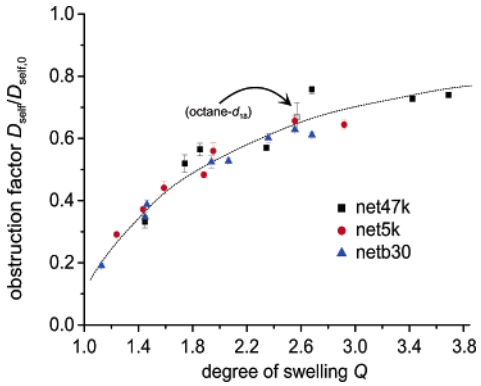

Figure 6. Results of PFG diffusion measurements of the swelling agent plotted in terms of an obstruction factor $D_{self}/D_{self,0}$, where $D_{self,0} = 2 \times 10^{-9}$ m^2/s for octane at 297 K. The error bars indicate the variation of D_{self} determined at different diffusion times, Δ. The line is simply a guide to the eye.

$$m = [\langle \mathbf{b}\rangle^2]/[\langle b^2\rangle] \tag{6}$$

We take every bond vector to belong to a chain composed of N freely fluctuating bonds with *fixed* end-to-end distance $\mathbf{R} = \sum_{k=1,N} \mathbf{b_k}$, where the index k denotes the bond number within a given chain. When we assume that the averaged bond vector does not vary along the chain (which is true for Gaussian chain statistics), we immediately obtain $\langle \mathbf{b}\rangle = \langle \mathbf{R}\rangle/N$ and hence

$$m = \frac{[\mathbf{R}^2]}{N^2[\langle b^2\rangle]} \tag{7}$$

We can further assume that $[\langle b^2\rangle]$ is the squared statistical bond length and that it is the same for all monomers. We thus write $b^2 = [\langle b^2\rangle]$. We use this simplified notation in the following; however, we always calculate the averages directly for different sets of bonds considered. When the cross-linking process proceeds in a way that it freezes-in an actual Gaussian distribution of end-to-end vectors of the precursor chains, one obtains $[\mathbf{R}^2] = Nb^2$ and hence

$$m^{\mathrm{Gauss}} = 1/N \tag{8}$$

Note that this result is independent of any details of the actual distribution function of bond orientations. In particular, eq 7 is also valid for non-Gaussian chain statistics. The order parameter m thus reflects the mean (orientational) order of the polymer segments independent of any fluctuation properties.

The autocorrelation function $m(t)$, given by eq 5, is displayed in Figure 7 for various sets of bonds. To avoid contributions from dangling parts or small loops (large loops are rare and very likely to be entangled), we remove all those chains from the gel part. The remaining set of monomers is called the purified part of the network. Note that in the NMR experiments purifying corresponds to the subtraction of the slowly relaxing

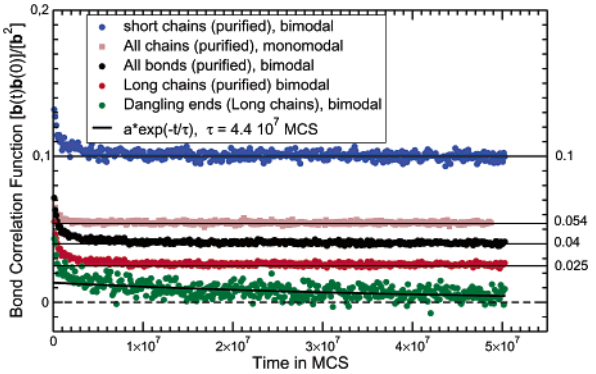

Figure 7. Autocorrelation function of bond vectors for various sets of chains in unswollen mono- and bimodal networks. The purified part of the networks is obtained by removing loops and dangling ends from the gel part. The long time limits of the correlation functions are indicated on the right.

Table 3. Simulated Order Parameters and Stretching Ratios, As Defined in the Text, Evaluated at the End of the Simulation Time and Comparison with Predictions from Theory

	monomodal	bimodal (short/long)
m (dry)	0.054	0.04 (0.1/0.025)
m (swollen)	0.143	0.113 (0.22/0.086)
λ_m	2.65	2.85 (2.16/3.44)
(5/3)s (dry)	0.055	0.048 (0.084/0.038)
(5/3)s (swollen)	0.12	0.1 (0.2/0.072)
λ_s	2.18	2.08 (2.38/1.9)
$m^{\text{Gauss}} = (5/3)s^{\text{Gauss}}$ [a]	0.038	0.04 (0.17/0.01)
$\lambda_m^{\text{affine}} = \lambda_s^{\text{affine}}$ [b]	2.77	2.87

[a] Equations 8 and 13 for dry networks. [b] Equation 10.

"tails" from the sum intensity, which are associated with (almost) isotropically reorienting segments.

The initial relaxation behavior of $m(t)$ exhibits some peculiarities. According to the Rouse model, $m(t)$ should decay exponentially, dominated by the longest (Rouse) relaxation time. This is roughly fulfilled for the monomodal network and the long chains in the bimodal network. However, the order parameter for the short chain subnetwork displays a relaxation which is much slower than expected (some 1000 MCS). This observation concurs with the fact that the order parameter of the set of short chains (see below) is lower than expected, probably due to *fast, cooperative motions* of clusters of short chains.[20] Such motions would introduce additional, longer time scales, in agreement with the observation. A closer analysis reveals that after a rapid decay on the time scale of about 5 000 000 MCS there is still a very weak, slower decay of the order parameter (observable on a logarithmic time scale). Thus, the order parameters reported here do not fully correspond to equilibrium values but are at least close to it. Finally, we observe that the dangling ends (long chains only) also display an additional, rather slow relaxation, which is now clearly apparent on the time scale chosen in Figure 7. An exponential fit yields a relaxation time of about 4.4×10^7 MCS; it most probably corresponds to reptation-like arm retraction processes.

Long-time limit order parameters and comparisons to eq 8 are listed in Table 3. One notable observation is that m for both the monomodal network as well as the long chains in the bimodal network exceeds the theoretical predictions. A straightforward explanation might embody the influence of (trapped) entanglements, which increase orientational order. Moreover, m for the monomodal network is larger than the average value for all chains in the bimodal network, although the latter has on average an even smaller effective strand length. In contrast, m for the short-chain subnetwork is much *lower* than expected. (Note that the Gaussian approximation is not too bad even for these short chains[20] and that local stiffness would even increase the expected value.) Thus, additional large-scale fluctuations of cross-links reduce orientational order here. Considering these observations, we must conclude that m cannot be simply related to the averaged cross-link density but depends on details of the network topology.

To analyze the impact of swelling on segmental order, we define the stretching ratio of the order parameter λ_m as

$$\lambda_m = \frac{m(\text{dry})}{m(\text{swollen})} \tag{9}$$

By taking into account a simulation-inherent bond stretching due to swelling, the affine stretching ratio of the order parameter order, $\lambda_{\text{m}}^{\text{affine}}$, due to isotropic swelling according to eq 7 is given by

$$\lambda_{\text{m}}^{\text{affine}} = Q^{2/3}/\lambda_{\text{b}}{}^2 \quad \text{with } \lambda_{\text{b}}{}^2 = b_{\text{s}}{}^2/b_{\text{d}}{}^2 \tag{10}$$

where $b_{\text{s}}{}^2$ and $b_{\text{d}}{}^2$ denote the averaged squared bond length for the swollen and the dry system, respectively (Table 2). The bond correlation functions of the swollen networks have the same qualitative appearance as in the dry state (Figure 7), however with increased long-time limits. The results for the order parameter stretching are indicated in Table 3. While the average stretching rations for the mono- and bimodal networks are only slightly subaffine, we note serious discrepancies for the individual components of the bimodal network, where the short chains transform subaffinely, while the long ones stretch superaffinely. Yet, our previous investigations have shown that the long chains are not overstretched concerning their end-to-end distance but deform slightly subaffinely.[20] These findings are further not in agreement with the NMR observations presented above.

In NMR experiments, the intuitive autocorrelation function of bond vectors cannot directly be obtained. Instead, the tensor order parameter $\mathbf{S}$ plays the fundamental role and controls the effect of motion-averaged dipole−dipole interactions. $\mathbf{S}_k$ for a single segment may be defined as

$$S_k^{\alpha\beta}(t) = \langle e_k^{\alpha}\, e_k^{\beta} \rangle - \frac{1}{3} \tag{11}$$

where the Greek indices denote the spatial components and $\mathbf{e}_k$ denotes the normalized bond vectors. The average is taken over the time passed during the experimental observation. Thus, it corresponds to a running average instead of a correlation function as defined in eq 5. On the other hand, $\mathbf{S}_k$ defines an orientational order also in the absence of a vector orientation of geometrical objects: $\mathbf{S}_k$ is invariant with respect to a change of sign of $\mathbf{e}_k$. From $\mathbf{S}_k$, we extract a scalar order parameter s defined as

$$s(t) = \left[\sqrt{\frac{3}{2}\text{Tr}\{\mathbf{S}^2(t)\}}\right] \tag{12}$$

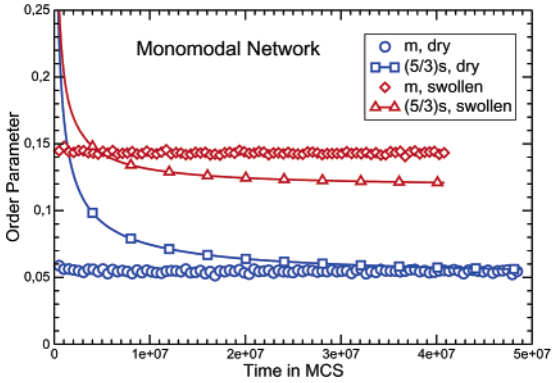

Figure 8. Comparison between $m(t)$ and $s(t)$ for all bonds in the purified part of the monomodal network. Here, we have rescaled $s(t)$ by a factor of $^5/_3$, as suggested by eq 13.

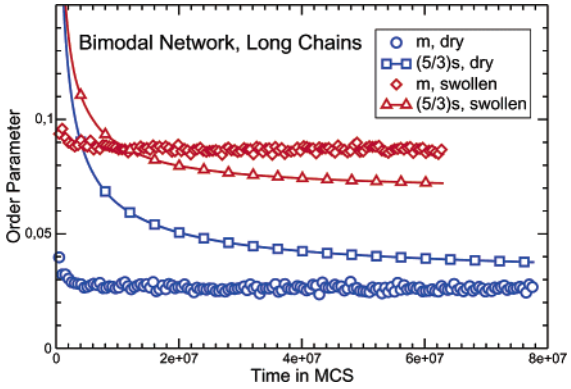

Figure 9. Same as in Figure 8, but for the bimodal network.

where the symbols [...] denote again the average over a given set of bond vectors. For Gaussian chains with fixed end-to-end distance **R**, we obtain in the limit of long times ($s = s(t \to \infty)$)

$$s^{\text{Gauss}} = \frac{3}{5}\left(\frac{[R^2]}{N^2b^2}\right) = \frac{3}{5}\frac{1}{N} = \frac{3}{5}m^{\text{Gauss}} \qquad (13)$$

in agreement with the traditional interpretation of NMR data represented by eq 1. Two remarks are essential at this point. First, the tensor order parameter, unlike its vector-like counterpart, is *not independent of the fluctuation statistics* of the bond vectors. This can be seen by considering the average tensorial order parameter for all bonds in a given chain, which reads $[\mathbf{S}] = (1/N)\sum_{k=1,N}\mathbf{S}_k$. Here, a sum of squares of bond vectors has to be averaged (see eq 11), which cannot simply be reduced to the actual end-to-end distance vector **R**. In fact, eq 13 depends strongly on the Gaussian chain distribution. (For instance, a lattice model would yield a different prefactor, usually larger than $^3/_5$.) Second, the running time average of $s(t)$ gives rise to a power-like relaxation behavior which may mask the true relaxation of orientational order. To understand the latter effect, consider a unit vector **e** which randomly orients in the coordinate directions of a simple two-dimensional lattice. There are only two different realizations for an actual **S**, corresponding to the two orientations in the x and y directions:

$$\mathbf{S}_x = \begin{pmatrix} \frac{1}{2} & 0 \\ 0 & -\frac{1}{2} \end{pmatrix} \quad \text{and} \quad \mathbf{S}_y = \begin{pmatrix} -\frac{1}{2} & 0 \\ 0 & \frac{1}{2} \end{pmatrix} \qquad (14)$$

The sum of randomly taken successions of $\mathbf{S}_x$ and $\mathbf{S}_y$ yields a random walk for each diagonal component, and the mean amplitude of each walk grows with $\sqrt{t}$. If we normalize the average by the number of averaging steps, t, we can easily see that the components of **S** decrease according to $t^{-1/2}$, and so does $s(t)$. This result is most important for computer simulations in which discrete steps are used to calculate the averages.

In Figure 8, we compare the relaxation behavior of the tensor order parameter, $s(t)$, with the vector order parameter, $m(t)$, for the monomodal network. In the dry state, eq 13 is well approached (although equilibrium is not yet fully reached). However, both order parameters differ considerably in the swollen state. The tensor order parameter approaches a much lower value than $m(t)$. This is a general consequence of the fluctuation dependence of s! A similar result is obtained for the bimodal network.

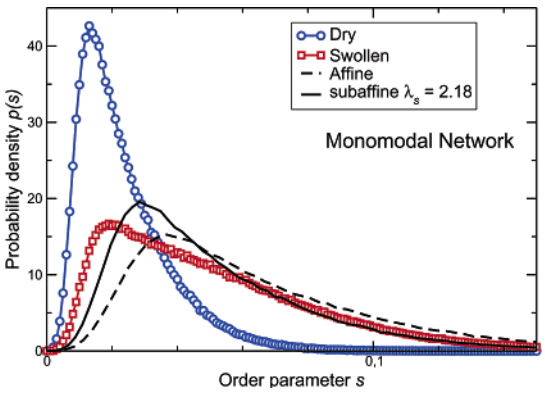

Figure 10. Distribution of the tensor order parameter for all bonds in the purified set of the monomodal network. The value of s is evaluated at the end of the simulation time.

It is particularly interesting to analyze the set of long chains separately (bimodal network), as shown in Figure 9. The values reached by the tensor order parameter are substantially higher in the dry state and lower in the swollen state. Thus, the tensor order parameter always exhibits a lower ratio λ_s as compared to λ_m after swelling. For long chains in the bimodal network, we obtain an average increase of order by only a factor of $\lambda_s = 1.9$, which is evidently subaffine, as opposed to the superaffine result for λ_m. This clearly shows the mixed character of the tensorial order parameter in comprising both orientational order and fluctuation properties of segments. Simulations of single, end-tethered chains show that the large deviations between the two order parameters cannot be explained by single chain effects. While without excluded volume m and $^5/_3 s$ match well, good solvent conditions lead to an only slightly decreased tensor order.

So far, we have considered averages of the order parameters for various sets of bonds. The great advantage of the tensor order parameter is its excellent statistics obtained for the individual bonds. For a comparison with the NMR results in the preceding section, we present the distribution of s, $p(s)$, for the case of the monomodal network in Figure 10. Clearly, the distribution broadens in the swollen state and cannot be reproduced by simple rescaling of the distribution of the dry state. Even using the subaffine averaged order parameter ratio of $\lambda_s = 2.18$, no coinci-

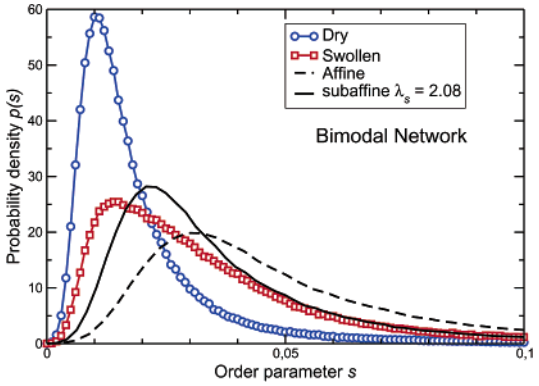

Figure 11. Distribution of the tensor order parameter obtained at the maximum simulation time for all bonds in the purified part of the bimodal network.

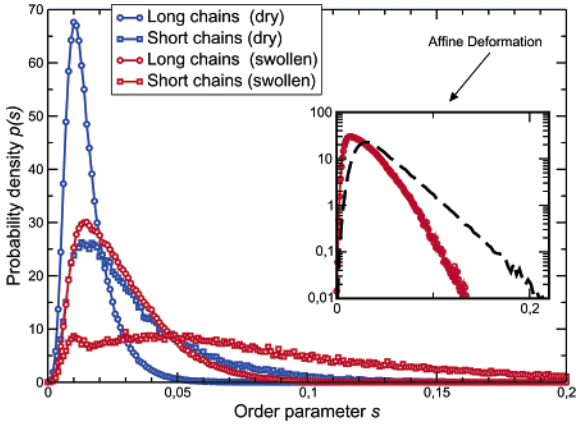

Figure 12. Separate distributions of the tensor order parameters in the bimodal network obtained at the swollen state compared with the affine transformation of the data obtained for the dry system.

dence between the rescaled distribution in the dry state and the actual distribution in the swollen state can be achieved.

The most remarkable observation concerns the maximum of the distribution function, which is only slightly shifted. This is compensated by the formation of a shoulder in the swollen state which does not exist in the dry state. Thus, the average increase of order originates mainly from the broadening of the distribution. We therefore see strong indications for an inhomogeneous swelling process, in which certain sets of chains are less deformed while other parts are more strongly deformed. For a direct observation of inhomogeneous swelling in bimodal networks as well as nonaffine deformations of the network strands, we refer to our previous work.[20]

In Figure 11, we show the distribution of the tensor order parameter averaged over all bonds in the purified part of the bimodal network, in which the bimodality is only reflected in a weak shoulder at higher values of $s > 0.05$. As in the case of the monomodal network, the maximum of the order parameter distribution does not follow the average but is shifted much less.

Additional insight is gained by a separate analysis for the two types of chains in the bimodal network (Figure 12). Again, the maxima of the distributions are only slightly shifted upon swelling (by less than a factor of 1.2 for the long chains). Of particular interest is $p(s)$ for the short chains in the swollen state, where two peaks are apparent. The first peak can be associated with small clusters of short chains which can reorient almost isotropically. This coincides with our observation of a low m in Figure 7 and again indicates a high mobility of short chains in such a network, where cooperative motions are apparently facilitated in the swollen state. The second peak corresponds to chains that are overstretched in the swelling process. Thus, also here, orientational order develops clearly inhomogeneously upon swelling.

IV. Discussion

A. Comparison of NMR and Simulation Results. The central and most convincing observation when comparing the results from MQ NMR (Figure 4) and computer simulations (Figures 10−12) is the agreement concerning the significantly increasing width of the (tensor) order parameter distributions upon swelling as well as the clear-cut subaffine behavior of these distributions. Both experiments and simulations display a highly subaffine shift of the maxima of the distributions, and the picture of an unfolding or desinterspersion process might apply for the understanding of such a behavior. The shift of the maximum can even become negative in the experimental case, probably due to different (lower) solvent quality and the consequently lower swelling ratios. Most importantly, as perceived from experimental as well as simulation results of the monomodal systems, a broadening of the order parameter distributions indicates heterogeneous ordering (deformation) processes during swelling. This furnishes new evidence for the existence and nature of swelling heterogeneities and the importance of complex, topological rearrangements.

In addition, we have found that the traditional interpretation of NMR results in terms of residual orientational order, eq 1, is not fully correct. While the vector order parameter m is practically independent of fluctuation statistics of the chains (and is therefore a direct measure of true orientational order), the experimentally accessible tensor order parameter s combines orientational order with fluctuation effects. Different distribution functions for the segment orientations can lead to different long-time limiting values of s. Considering its fluctuation dependence, swelling has two effects. First, segments become more oriented, leading to an increase of s. Second, fluctuations are enhanced, leading to a decrease of s. Additional single-chain simulations (to be published elsewhere) have shown that solvent effects alone can hardly explain the large deviations between m and s in a network. In this regard, the role of entanglement constraints and the development of interchain orientational correlations (packing constraints) upon swelling will have to be addressed in more detail.

Qualitative agreement of the distributions by NMR and simulations can also be reported for the two components of the bimodal networks (Figure 4d, Figure 12, and Table 3), where the tensorial order of the long chains is seen to increase much less upon swelling than that of the short chains. Note that the bimodality of the simulated distributions is not as clear-cut as in the experiment, since the difference in length between short and long chains is not as big as in the experiment, and the experimental swelling degree is not as high as in the simulation.

The average values of S_b for dry net47k ($N = 109$, see Table 1) as well as the long-chain component of

netb30 of about 3 are also in good agreement with the simulation result for the long chains in the bimodal network. Their relatively high values of about 3% cannot be accounted for by a simple $1/N$ relationship, indicating the significance of trapped entanglements or mutual chain packing. This observation is not challenged by the fluctuation dependence of tensorial order, as it is also supported by the bond autocorrelation function calculated for the simulated networks. The sample with medium-size chains, net5k, features an experimental S_b of 0.06, while the value expected from $N = 12$ is 0.05, also in agreement with less serious deviations observed in the simulations of the monomodal network.

Concerning the very short chains in the mono- and bimodal networks, in our previous work[39] we have already discussed the deviations of experimental values of N (4−6, as calculated from the residual couplings using eq 1) from the expected value of 2 in terms of possible chain elongation during cross-linking. In light of simulation data presented herein, we conclude that this deviation should to a significant degree be due to large-amplitude cooperative motions of short-chain clusters and details of the fluctuation processes. Note that the lower value of around 4 is found for pure net800 ($D_{avg}/2\pi = 700$ Hz, $S_b = 0.16$), which could be due to chain elongation, while for netb30, $N \approx 6$ ($D_{avg}/2\pi = 450$ Hz, $S_b = 0.1$), indicating additional orientational averaging by fast cross-link reorientations.

B. Time Scales of Tensor Averaging. An important issue concerning the tensor order parameter is its time dependence resulting from the self-averaging processes. In practice, these processes are assumed to correspond to fast-motion averaging of segment orientations during the NMR measurement. In the simulations, however, a power-law decay of $s(t)$ with surprisingly slow dynamics toward true equilibrium averages becomes apparent (Figures 8 and 9) and might challenge the fast-motion assumption (which appears clearly valid for $m(t)$).

An important question to ask is therefore how far the long simulation time limit, at which the (residual) tensor order parameter is evaluated, is related to the experimental NMR time scale. From the Rouse diffusion coefficient of a PDMS melt given in ref 60, we obtain a room temperature value for the diffusion constant of a single Kuhn segment: $D_R N = kT/\zeta \approx 186$ Å^2/ns. With a mean-square displacement by a single Kuhn segment size, $b^2 = (5.6$ Å$)^2$,[44] a characteristic displacement time of 0.17 ns can be estimated. In BFM, a segmental displacement usually takes around 100 MCS, such that a simulation time of 50 000 000 MCS corresponds to about 0.1 ms real time, which is of the same order of magnitude as the NMR time scale defined by $2\pi/D_{stat}$. However, the initial decay of $s(t)$ ocurrs within a much shorter time (Figure 8), and the experimental order parameters should therefore be close to the simulated values, with the fast-motion assumption being applicable.

Since the NMR results are independent of temperature over tens of kelvin,[39] it seems reasonable to conclude that NMR measures the long-time plateau of $s(t)$. The ongoing weak power-like decay of the tensor order parameter on the experimental time scale apparently exerts only minor influence on the normalized DQ buildup (in which such slow-motion effects are partially compensated for). Yet, the long-time decays of integral intensities in MQ experiments (as well as specific shapes of relaxation functions in traditional experiments) are usually interpreted in terms of slow reorientations of the residual dipolar tensor attributed to restricted, cooperative fluctuations of the cross-links.[40] Our finding of a slow power-like slow decay of $s(t)$ might also suggest a superposition of long time relaxation processes with the relaxation process identified herein, which emerges from the averaging procedure. We note that here a direct link between the formally averaged order parameter defined by eq 11 and the quantum-mechanical averaging during random bond rotations has to be established first. Further work along these lines is in progress.

C. Comparison with Previous NMR Work. The results for the three monomodal networks reported here are not in good agreement with previous NMR studies based on fits to relaxation functions. In swollen PDMS[29,30] as well as polyethylene networks,[31] a fitting parameter which is supposedly related to the average residual coupling also exhibits a clearly nonaffine behavior, yet its value goes through a minimum at a volume swelling of $Q \approx 2-3$, which was interpreted in terms of strong chain desinterspersion effects.

Assuming mutual chain packing as the origin of the increase the order parameter of the dry networks, topological unfolding processes in combination with dilution by solvent lead to an increase in overall chain mobility. Such unfolding or desinterspersion processes can occur without appreciable changes in the overall dimension of topologically restricted subchains[6,32] and are clearly supported by our simulations, in particular by considering the difference between tensor and vector order parameters. While the latter accounts for the effect of entanglement constraints during swelling, the former indicates the (dramatic) fluctuation enhancement in the swollen state which is clearly observed in the experiments.

We should mention that all the networks used herein have on average less than 5% liquidlike components (residual sol and dangling chains). Other strategies for the synthesis of networks, such as, e.g., end-linking by hydrosilylation of divinyl-terminated PDMS chains, may easily lead to much higher liquidlike contents.[29,31,61] In relaxation decay experiments, these components may not be as reliably separable from the network response as in our MQ approach, simply because an intensity buildup is inevitably associated with dipolar coupled segments only. Moreover, none of the models used to interpret relaxation decays take distributions into account, which might bias the fitting result. Note that one-component fits to our data (crosses in Figure 5a−c) show marked deviations from the average residual couplings; i.e., the so-obtained values do exhibit a slight decrease rather than an increase over the investigated range. This might represent another possible reason why our results differ from the previous relaxation studies.

We could imagine the possibility that, upon swelling, a Gaussian distribution of end-to-end distances between constraints is restored, which is supported by the results for simulated networks presented in ref 19. The buildup curve for net47k swollen to near equilibrium (Figure 3) resembles the buildup function calculated under the assumption of Gaussian statistics published previously.[39] While this would be in agreement with the desinterspersion picture, in which chain packing in the dry state might be responsible for the rather narrow distribution observed for net47k,[39] we note, however, that a Gaussian distribution of end-to-end distances of

(long) chains does not necessarily imply Gaussian statistics on smaller length scales such as the distribution of segment orientations.

V. Summary and Conclusions

We have performed MQ NMR as well as computer simulations to investigate the dynamics and local distribution of segmental order upon swelling of end-linked PDMS and BFM networks. In both approaches, we have observed qualitatively the same results of significant, clearly nonaffine increases in the width of the order parameter distributions upon swelling. These are indicative of substantial differences in the conformational freedom of chain segments subject to topological constraints, providing evidence that swelling is a heterogeneous process related to motions on length scales larger than the averaged strand length. In addition, the average chain order parameters do not follow the affine prediction.

Our analysis of the simulated systems permits the investigation of both vector and tensor order parameters. We have shown that neither the average of the tensor order parameter probed by NMR nor the simulated vector order parameter might correctly reflect end-to-end separations of subchains. In particular, for the tensor order parameter, freely rotating segments (or Gaussian statistics in a continuous description) as an essential assumption of established models are not necessarily present. While the vector order parameter (long-time limit of the segment-vector autocorrelation function) correctly describes residual orientational order of the segments, the tensor order parameter is sensitive to additional changes in the local orientation distributions. The strongly subaffine behavior of the tensor order parameter is partially related to a rather dramatic change in the fluctuation statistics. Our findings can be explained in terms of a chain desinterspersion process in which at the early stages of swelling chain segments between topological constraints acquire a higher mobility due to a release of mutual chain packing upon swelling. The observation of a significantly increased tensor order parameter for long chains in the dry state indicates additional dynamic correlations between segments of entangled chains, which deviate from the Gaussian prediction. These issues will be dealt with in more detail in forthcoming work.

Finally, as to the spatial extension of the observed chain order heterogeneities, our diffusion results do not yield conclusive information on their length scale. On one hand, we are planning to extend our diffusion studies to larger probe molecules, for which ultimately a stronger diffusion contrast and an enhanced effect on time, space, and q dependence of the diffusion coefficient is expected.[62] On the other hand, having established the close correspondence of experimental results and computer simulations, we are confident that detailed information on the spatial correlation of different components in the order parameter distribution will result from our ongoing in-depth analysis of the computer-simulated networks.

Acknowledgment. The authors thank A. Vidal, B. Haidar, P. Ziegler, and O. Spyckerelle for the PDMS network samples. Funding was provided by the Landesstiftung Baden-Württemberg, the Deutsche Forschungsgemeinschaft (SFB 428), and the Fonds der Chemischen Industrie.

References and Notes

(1) Flory, P. J.; Rehner, J., Jr. *J. Chem. Phys.* **1947**, *11*, 512.
(2) Sperling, L. H. *Physical Polymer Science*; John Wiley & Sons: Danvers, 2001.
(3) Brotzmann, R. W.; Eichinger, B. E. *Macromolecules* **1981**, *14*, 1445.
(4) Gottlieb, M.; Gaylord, R. J. *Macromolecules* **1984**, *17*, 2024.
(5) Neuburger, N. A.; Eichinger, B. E. *Macromolecules* **1988**, *21*, 3060.
(6) Bastide, J.; Picot, C.; Candau, S. *J. Macromol. Sci., Phys.* **1981**, *B19*, 13.
(7) Bastide, J.; Leibler, L. *Macromolecules* **1988**, *21*, 2647.
(8) Ullman, R. *Macromolecules* **1982**, *15*, 582.
(9) Mallam, S.; Horkay, F.; Hecht, A.-M.; Geissler, E. *Macromolecules* **1989**, *22*, 3356.
(10) Mendes, E., Jr.; Lindner, P.; Buzier, M.; Boué, F.; Bastide, J. *Phys. Rev. Lett.* **1991**, *66*, 1595.
(11) Mallam, S.; Horkay, F.; Hecht, A.-M.; Rennie, A. R.; Geissler, E. *Macromolecules* **1991**, *24*, 543.
(12) Mendes, E.; Girard, B.; Picot, C.; Buzier, M.; Boué, F.; Bastide, J. *Macromolecules* **1993**, *26*, 6873.
(13) Soni, V. K.; Stein, R. S. *Macromolecules* **1990**, *23*, 5257.
(14) Shibayama, M. *Macromol. Chem. Phys.* **1998**, *199*, 1.
(15) Hirokawa, Y.; Jinnai, H.; Nishikawa, Y.; Okamoto, T.; Hashimoto, T. *Macromolecules* **1999**, *32*, 7093.
(16) Panyukov, S.; Rabin, Y. *Phys. Rep.* **1996**, *269*, 1.
(17) Rabin, Y.; Panyukov, S. *Macromolecules* **1997**, *30*, 301.
(18) Sommer, J. U.; Vilgis, T. A.; Heinrich, G. *J. Chem. Phys.* **1994**, *100*, 9181.
(19) Sommer, J. U.; Russ, T.; Brenn, B.; Geoghegan, M. *Europhys. Lett.* **2002**, *57*, 32.
(20) Sommer, J.-U.; Lay, S. *Macromolecules* **2002**, *35*, 9832.
(21) Escobedo, F.; de Pablo, J. *Phys. Rep.* **1999**, *318*, 85.
(22) Pütz, M.; Kremer, K.; Everaers, R. *Phys. Rev. Lett.* **2000**, *84*, 298.
(23) Sommer, J.-U. *Macromol. Symp.* **1994**, *81*, 139.
(24) Hölzl, T.; Trautenberg, H.; Göritz, D. *Phys. Rev. Lett.* **1997**, *79*, 2293.
(25) Hölzl, T.; Trautenberg, H.; Göritz, D. *Phys. Rev. Lett.* **1999**, *82*, 1342.
(26) Schmidt-Rohr, K.; Spiess, H. W. *Multidimensional Solid-State NMR and Polymers;* Academic Press: London, 1994.
(27) Cohen-Addad, J. P. *J. Chem. Phys.* **1973**, *60*, 2440.
(28) Cohen-Addad, J. P. *Prog. NMR Spectrosc.* **1993**, *25*, 1.
(29) Cohen-Addad, J. P.; Domard, M.; Herz, J. *J. Chem. Phys.* **1982**, *76*, 2744.
(30) Cohen-Addad, J. P.; Domard, M.; Lorentz, G.; Herz, J. *J. Phys. (Paris)* **1984**, *45*, 575.
(31) Schmit, C.; Cohen-Addad, J. P. *Macromolecules* **1989**, *22*, 142.
(32) Deloche, B.; Samulski, E. T. *Macromolecules* **1988**, *21*, 3107.
(33) Cohen-Addad, J. P. *J. Chem. Phys.* **1975**, *63*, 4880.
(34) Gotlib, Y. Y.; Lifshitz, M. I.; Shevelev, V. A.; Lishanskij, I. S.; Balanina, I. V. *Vysokomol. Soedin. A18* **1976**, *10*, 2299.
(35) Collignon, J.; Sillescu, H.; Spiess, H. W. *Colloid Polym. Sci.* **1981**, *259*, 220.
(36) Callaghan, P. T.; Samulski, E. T. *Macromolecules* **1997**, *30*, 113.
(37) Fischer, E.; Grinberg, F.; Kimmich, R.; Hafner, S. *J. Chem. Phys.* **1998**, *109*, 846.
(38) Fechete, R.; Demco, D. E.; Blümich, B. *J. Chem. Phys.* **2003**, *118*, 2411.
(39) Saalwächter, K.; Ziegler, P.; Spyckerelle, O.; Haidar, B.; Vidal, A.; Sommer, J.-U. *J. Chem. Phys.* **2003**, *119*, 3468.
(40) Saalwächter, K. *J. Chem. Phys.* **2004**, *120*, 454.
(41) Saalwächter, K. *J. Am. Chem. Soc.* **2003**, *125*, 14684.
(42) Graf, R.; Heuer, A.; Spiess, H. W. *Phys. Rev. Lett.* **1998**, *80*, 5738.
(43) Schneider, M.; Gasper, L.; Demco, D. E.; Blümich, B. *J. Chem. Phys.* **1999**, *111*, 402.
(44) Beaucage, G.; Sukumaran, S.; Clarson, S. J.; Kent, M. S.; Schaefer, D. W. *Macromolecules* **1996**, *29*, 8349.
(45) Bercea, M.; Cazacu, M.; Wolf, B. A. *Macromol. Chem. Phys.* **2003**, *204*, 1371.
(46) Kuhn, W.; Grün, F. *Kolloid-Z.* **1942**, *101*, 248.
(47) Sotta, P.; Fülber, C.; Demco, D. E.; Blümich, B.; Spiess, H. W. *Macromolecules* **1996**, *29*, 6222.
(48) Baum, J.; Pines, A. *J. Am. Chem. Soc.* **1986**, *108*, 7447.
(49) Saalwächter, K.; Klüppel, M.; Luo, H.; Schneider, H. *Appl. Magn. Reson.,* in press.
(50) Weese, J. *Comput. Phys. Commun.* **1992**, *69*, 99.
(51) Tanner, J. E. *J. Chem. Phys.* **1970**, *52*, 2523.
(52) Price, W. S. *Concepts Magn. Reson.* **1997**, *9*, 299.

(53) Carmesin, I.; Kremer, K. *Macromolecules* **1988**, *21*, 2819.
(54) Paul, W.; Binder, K.; Kremer, K.; Heermann, D. W. *Macromolecules* **1991**, *24*, 6332.
(55) Sotta, P.; Deloche, B. *Macromolecules* **1990**, *23*, 1999.
(56) Callaghan, P. T. *Principles of Nuclear Magnetic Resonance Microscopy*; Oxford University Press: Oxford, 1993.
(57) Fechete, R.; Demco, D. E.; Blümich, B. *Macromolecules* **2003**, *36*, 7155.
(58) Yamane, Y.; Kobayashi, M.; Kuroki, S.; Ando, I. *Macromolecules* **2001**, *34*, 5961.
(59) Hecht, A. M.; Guillermo, A.; Horkay, F.; Mallam, S.; Legrand, J. F.; Geissler, E. *Macromolecules* **1992**, *251*, 3677.
(60) Arbe, A.; Monkenbusch, M.; Stellbrink, J.; Richter, D.; Farago, B.; Almdal, K.; Faust, R. *Macromolecules* **2001**, *34*, 1281.
(61) Sotta, P. *Macromolecules* **1998**, *31*, 3872.
(62) Russ, T.; Brenn, R.; Abel, F.; Boué, F.; Geoghegan, M. *Eur. Phys. J. E* **2001**, *4*, 419.

MA048803K